Mat. Res. Soc. Symp. Proc. Vol. 737 © 2003 Materials Research Society E17.1.1

Size and shape dependent level structure in CdSe quantum rods

Eli Rothenberg[1], Taleb Mokari[1], Uri Banin[1], David Katz[2], Tommer Wizansky[2], and Oded Millo[2]
[1]Institute of Chemistry, and the Center for Nanoscience and Nanotechnology,
The Hebrew University of Jerusalem, Jerusalem 91904, Israel
[2]Racah Institute of Physics and the Center for Nanoscience and Nanotechnology,
The Hebrew University of Jerusalem, Jerusalem 91904, Israel

ABSTRACT

Optical spectroscopy and Scanning Tunneling Microscopy are used to study the size and shape dependence of the electronic states in CdSe quantum rods. The quantum rods were grown using colloidal chemistry synthesis methods, with good control over size and size distribution. Samples having average rod dimensions ranging from 10 to 60 nm in length and 3.5 to 7 nm in diameter, with aspect ratios varying between 3 to 12, were investigated. Both optical (at 10 K) and tunneling (at 4.2 K, on single rods) spectra show that the level structure depends primarily on the rod diameter and not on length. With increasing diameter, the band gap and the excited state level spacings shifted to the red. The level structure is assigned using a multi-band effective-mass model, showing relatively good agreement with experiment. We shall also discuss the effect of single electron charging on the tunneling spectra, possibly reflecting the quantum rod level degeneracy.

INTRODUCTION

Colloidal semiconductor nanocrystals are a class of nanomaterials that manifest the transition from the molecular limit to the bulk solid-state regime [1,2], with significant potential for serving as building blocks of nano-devices in applications ranging from lasers [3,4] and opto-electronic devices [5] to biological fluorescence tagging [6]. Shape control of such colloidally prepared nanostructures has been recently achieved by modifying the synthesis to obtain rod shaped particles - quantum rods (QRs) [7]. QRs exhibit electronic and optical properties different than quantum dots (QDs). For example, unlike the spherical dots, QRs have linearly polarized emission as demonstrated recently by fluorescence measurements on single rods [8], leading also to polarized lasing [4]. Here we combine optical and tunneling spectroscopies and correlate them with a multi-band effective-mass model, to investigate the electronic level structure of CdSe quantum rods, and study its dependence on rod length and diameter. The study provides significant insight on the evolution of the electronic structure from zero dimensional QDs to one-dimensional quantum wires.

The combination of scanning-tunneling and optical spectroscopies has proven to be a powerful approach to decipher the level structure of spherical nanocrystal QDs [2,9]. While in the optical spectra, allowed valence band (VB) to conduction band (CB) transitions are detected [10,11], in tunneling spectroscopy the CB and VB states can be separately probed yielding complementary information on the level structure [9,12,13,14]. Such data can provide an important benchmark for theoretical models of the level structure in strongly quantum-confined nanostructures, as was demonstrated for spherical QDs [15,16]. Multi-band effective-mass approaches [10,11,17] and atomistic pseudo-potential theory [15] were both used to describe measured QD size-dependent level spectra. Recently, both multiband effective-mass theory and

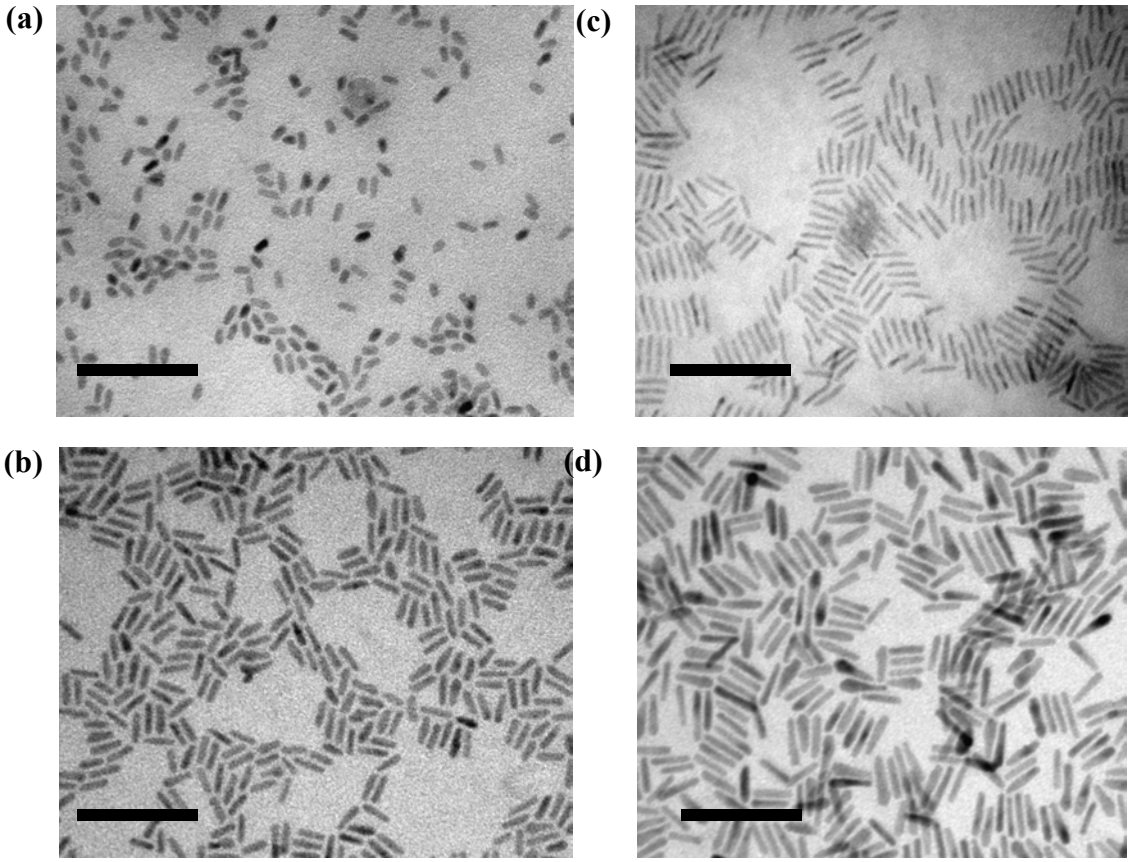

Figure 1. TEM images of four QR samples with average length x diameter, (a) 11x 5.5 nm, (b) 20 x 4.5 nm, (c) 29 x 3.7 nm, (d) 33 x 6.5 nm. Scale bar is 100 nm.

the pseudo-potential approach were applied for calculating the size dependent energy levels in QRs [18,19].

EXPERIMENTAL DETAILS

CdSe QRs were grown using the well-developed methods of colloidal nanocrystal synthesis, where the rods are overcoated by organic ligands [7,20,21]. The growth process was monitored by the absorption spectrum taken during the synthesis. Transmission electron microscopy (TEM) was used for size determination as well as to confirm the formation of rod shaped nanocrystals.

Low temperature (T = 10 K) optical spectroscopy was measured on QRs embedded in a free-standing polymer film, in particular size selective photoluminescence excitation (PLE) that probes the size dependent absorption level structure of nanocrystals. Here, one measures the excitation spectra using a narrow detection window on the blue side of the inhomogeneously broadened photoluminescence (PL) peak. The detection window selects a subset of the inhomogeneous sample, and structured excitation spectra are obtained. The measurements were carried out on different QR samples where the rod diameter and length were varied systematically.

For the scanning tunneling microscopy (STM) measurements, the QRs were spin-coated on highly oriented pyrolitic graphite (HOPG) substrate from a highly diluted QRs-hexane (or toluene) solution. The tunneling spectra (dI/dV vs. V characteristics) were obtained using the double barrier tunnel junction (DBTJ) configuration, by positioning the tip above a QR [14]. The data presented here were acquired with the tip retracted far away from the QR, thus suppressing single electron charging effects [13,14]. In addition, CB (VB) states appear at positive (negative) sample bias and the peak separations are close to the real QR level spacing. Moreover, as shown theoretically for QDs, the applied voltage does not affect much the level spectrum [16,22]. Hence, the dI/dV versus V spectra yield direct information on the QR level structure [12,13,14].

RESULTS

For the study of length and diameter dependence of the level structure, various QR samples were investigated having average dimensions ranging from 3.5 to 7 nm in diameter and from 10 to 60 nm in length. The variance of the rod dimensions within a given sample, as determined from TEM analysis, was 5 to 10% in diameter and 10 to 15% in length. Figure 1 presents four different QR samples exemplifying the good control over the QRs dimensions and size distribution.

In the low temperature optical experiments the samples exhibited absorption spectra with several transitions and a distinct PL peak assigned to band-gap emission (figure 2, left frame).

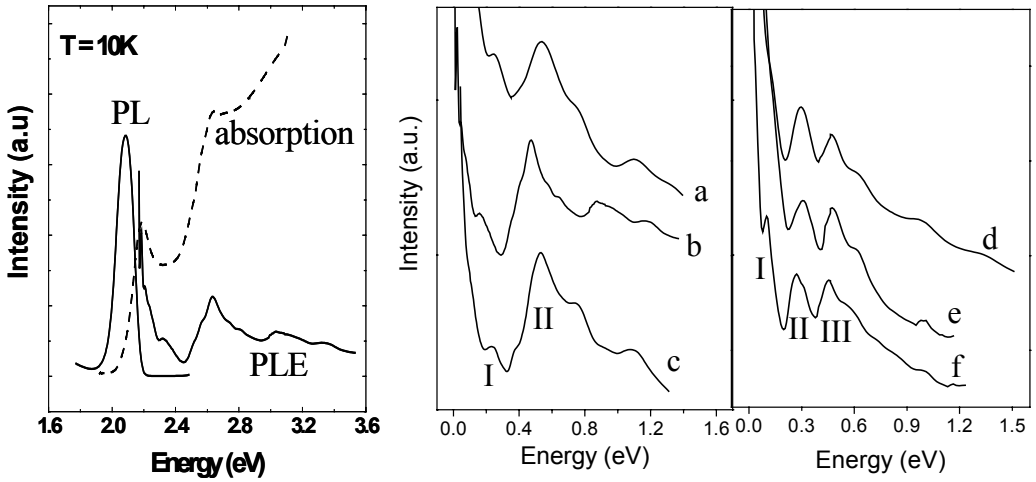

Figure 2. The left frame shows absorption, emission (PL) and size selective PLE spectra of a 21 x 3.7 nm QR sample. In the right frames, we plot PLE spectra obtained for six CdSe QR samples: (a) 31 x 3.8 nm (length x diameter on average), E_{det} = 2.25 eV (b) 21 x 3.7 nm, E_{det} = 2.16 eV (c) 11 x 3.2 nm, E_{det} = 2.25 eV (d) 60 x 6.7 nm, E_{det} = 2.00 eV (e) 30 x 6.5 nm, E_{det} = 2.01 eV (f) 11 x 5.8 nm, E_{det} = 2.03 eV, with the zero energy representing the position of the detection window, E_{det}. Relevant optical transitions are denoted as I, II and III. The structure above 0.7 eV is overlapping peaks of the excitation lamp that could not be completely normalized out.

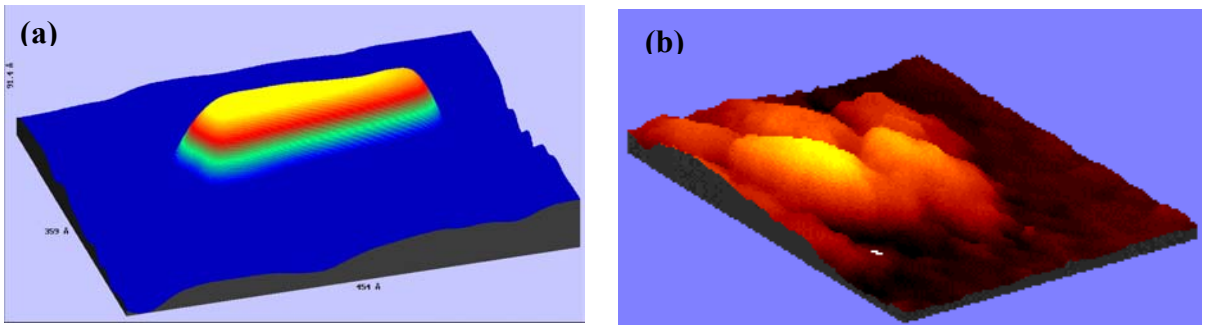

Figure 3. STM topographic images of (a) a *single* QR 25 nm long and 4 nm in diameter and (b) QRs aggregate.

The positions of the absorption onset and PL peak red shifted with increasing diameter and showed no significant variation with rod length (see figure 6) [23].

The PLE spectra presented in figure 2, were obtained, as explained above, by opening a narrow detection window at an energy E_{det} on the blue edge of the inhomogeneously broadened PL peak (figure 2, left frame) [10,11]. The spectra are less structured as compared with those measured on QDs due to the increased sources of inhomogeneous broadening in rods and due to the intrinsically less discrete level structure. A striking feature is the nearly identical level structure observed for the three QR samples of small diameter (traces a, b and c), which differs significantly from the spectra measured on the thicker rods (traces d, e and f), although in each group the aspect ratios vary from 3 to about 10. This shows clearly that not only the band-gap of the rods depends mainly on the diameter, but also the excited optical transitions.

The optical measurements were accompanied by STM measurements performed at T = 4.2 K on *single* QRs. Figure 3 presents STM topographical images of QRs deposited on the HOPG substrate. Single QRs were observed [figure 3 (a)] as well as clusters of QRs [figure 3 (b)] indicating their tendency to aggregate on the HOPG substrate.

Tunneling spectra measured on the QRs further demonstrate that the QR level structure depends primarily on the diameter of the QRs, not on their length, in accordance with the PLE data. One example of this behavior is presented in figure 4 (a), showing tunneling spectra for two QRs of different diameters and nearly the same length. Most significantly, upon comparing these two spectra, the region of suppressed tunneling conductance (null density of states) around zero bias, associated with the quasi-particle energy gap, is red shifted upon QR thickening from about 2.4 eV in the upper curve (d = 4 nm) to about 2.2 eV in the lower curve (d = 5.5 nm). This trend was not observed as clearly for the spacing between the CB ground state (CB1) and the first excited state (CB2), see figure 4(a). The weaker dependence on length compared with diameter was further observed in additional tunneling spectra as reported in Ref. 25.

Level CB3, appearing in the lower trace, was observed in about 50% of the measured rods, where the current did not reach the saturation limit before resolving this level. The VB is considerably more dense and complex and its level structure was not reliably resolved in our tunneling spectra; thus we only denote the first (ground state) peak as VB1 [figure 4(a)]. Further insight into the QR level structure, including the excited VB levels, is gained by correlating the tunneling spectra with allowed optical VB to CB transitions, and both measurements with theoretical calculation.

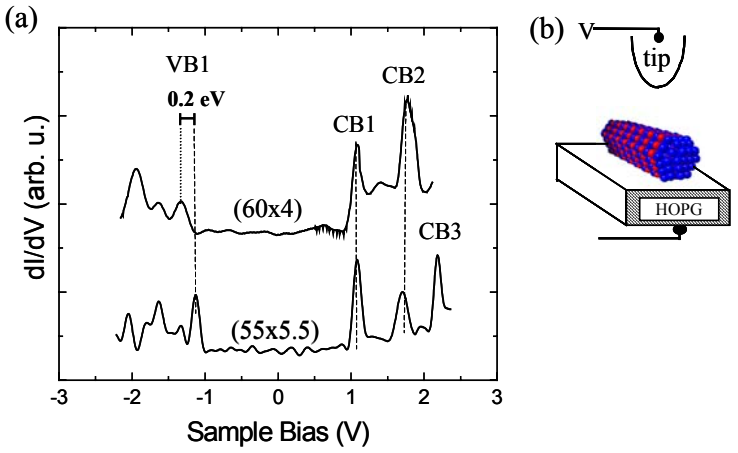

Figure 4. (a) dI/dV versus V tunneling spectra at 4.2 K for two QRs of dimensions (length x diameter) marked above each curve in nm. For clarity, the spectra were shifted horizontally to align the CB1 peaks. The vertical dashed lines are guides to the eye. The tunneling set values were in the range V_s = 1.5 – 2 V and I_s = 50 – 80 pA. (b) Schematic of the DBTJ configuration used for acquiring the tunneling spectra.

MODEL

An effective mass based approach was used in order to calculate the electronic structure of the QRs, following the formalism developed by Sercel & Vahala for quantum wires [24]. For aspect ratios larger than 3 as measured in our experiments it is reasonable to treat the confinement energy in the z axis as a perturbation. The same basis functions as in Ref. [24] were employed, using the following notation for the quantum numbers: n, the principal number, and F_z and L_z, the projections of the total and envelope angular momenta along the z axis, respectively. Here $F_z = J_z + L_z$ where J is the zone center Bloch angular momentum of the bulk bands. The finite length of the rods is expressed via an additional quantum number denoted by m, replacing the continuous wavevector k_z in Ref. 24, and accordingly a factor *exp(imz)* multiplies the eigenfunction.

The conduction-band states are calculated by using the uncoupled one-band model for a particle in a finite (U=5 eV) cylindrical potential-well. Figure 5 presents the first few CB energy levels with quantum number n, L_z and m. It is evident also from the model that the energy levels depend strongly on the rod radius [figure 5(a)], with a much weaker dependence on length [figure 5 (b)] in the regime studied here. This is due to the strong confinement in the small (radial) direction. Indeed, short rods approaching the bulk Bohr radius, or higher m states, effectively shortening the rods, do show significant length dependence. We denoted the conduction band states with m=1 as CB1, CB2 and CB3 according to the envelope function quantum number, L_z.

The VB states have been calculated using a four-band **k**·**p** model [24] which couples the heavy and light holes, in an infinite potential-well for F_z = 1/2, 3/2, 5/2. Calculated VB levels

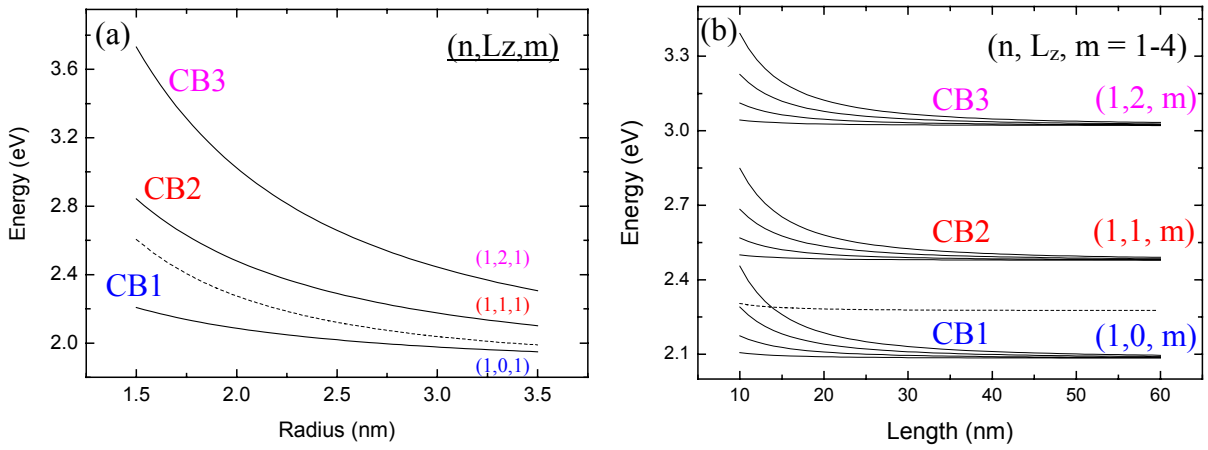

Figure 5. Conduction band energy levels of CdSe QRs calculated for a confining potential of 5 eV (solid lines). (a) First three energy states with m=1 versus QR radius, for a 30 nm long QR. The quantum numbers (n, L_z, m) are denoted. (b) Length dependence for the respective energy levels for a rod 2 nm in radius, showing also the dependence on the quantum number m. Dashed lines in both frame present the position of the ground state as calculated using an infinite potential well as in Ref. [25]. The energies are given with respect to the bulk VB edge. Effective-masses for electrons and the bulk energy gap were taken from Ref. [17].

are described in Ref. [25] where they were divided into three groups of closely spaced states denoted as VB1, VB2 and VB3. We note that each of these levels, and in fact each F_z level states contains contributions of various L_z components, resulting in weak selection rules.

DISCUSSION

In figure 6 we compare the measured optical transitions and tunneling spectra with the theoretical calculations. The gap extracted from the optical measurements (solid circles) and the gap identified in the tunneling data (empty squares), are plotted along with the calculated energy gap, VB1-CB1. In order to compare with the quasi-particle (tunneling) gap, the measured excitonic (optical) gap was corrected for the electron-hole Coulomb interaction.

As a first approximation, we modified the expression given in Ref. [26] for QDs, $1.8e^2/kr$ (where k is the dielectric constant), to take into account the fact that in our QRs strong confinement holds primarily for the radial dimension. We thus replace the radius, r, by $(r^2 a_0)^{1/3}$ where a_0 is the bulk CdSe Bohr radius, 5.7 nm. A relatively good agreement between the calculated and measured energy gaps is found for both tunneling and optical experiments. However, the tunneling gaps are higher in energy, as was previously observed for QDs [9]. This can be ascribed to the non-vanishing voltage drop on the QR-substrate junction, enlarging the measured level spacing [12,13,14] and to the overestimated QR radii measured by STM due to convolution with the tip [9].

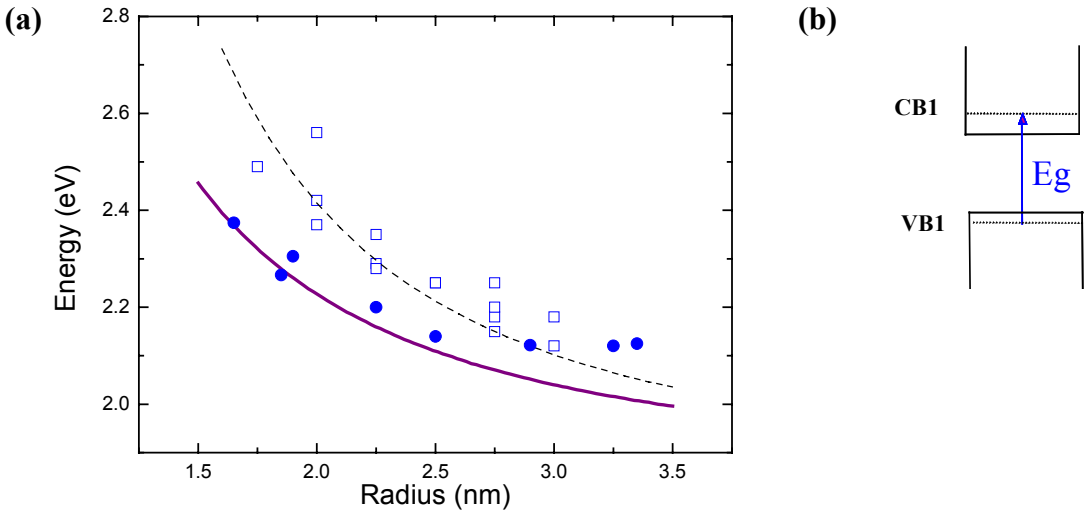

Figure 6. (a) Energy gap versus QR radius. The tunneling data (empty squares, size digitized due to uncertainty) and the model (solid and dashed lines represent finite and infinite potential wells, respectively) correspond to the energy separations VB1-CB1. The optical data (solid circles) were determined from the first absorption peak and corrected for the electron-hole Coulomb interaction, see text. (b) An illustration of the band-gap optical transition from VB1 to CB1.

Turning now to the excited levels, figure 7 shows spacings of the PLE transitions with respect to the band-gap transition, along with levels CB2 and CB3 measured with respect to CB1, detected by tunneling. The data are presented as a function of the band-gap measured in each experiment, thus eliminating the possible problem of QR radius estimation mentioned above. Most interesting is the agreement of the spacing between PLE transition II and the band-gap transition (solid squares) with the tunneling data for the CB2-CB1 level separation (open squares), both correlating well with the CB2-CB1 spacing. This allows the assignment of PLE peak II – to a transition between the VB ground state and CB2. Note that the calculated level spacing VB3-VB1 (upper dashed line) could also correspond to these PLE data, and thus peak II may also have contribution from the transition VB3-CB1. However the good correlation with the tunneling data provides significant support for the first assignment, manifesting the advantage of the combined optical-tunneling approach in deciphering the level structure. It is also clear from the good agreement with the model that PLE transition I (solid stars) takes place between the first excited VB state (VB2) and the CB ground state Transition III (solid circles) was resolved only for samples with larger diameters, and therefore cannot be clearly assigned yet. Considering again the tunneling data, figure 7 shows a weaker size (energy gap) dependence for CB2 and CB3 as compared to theory.

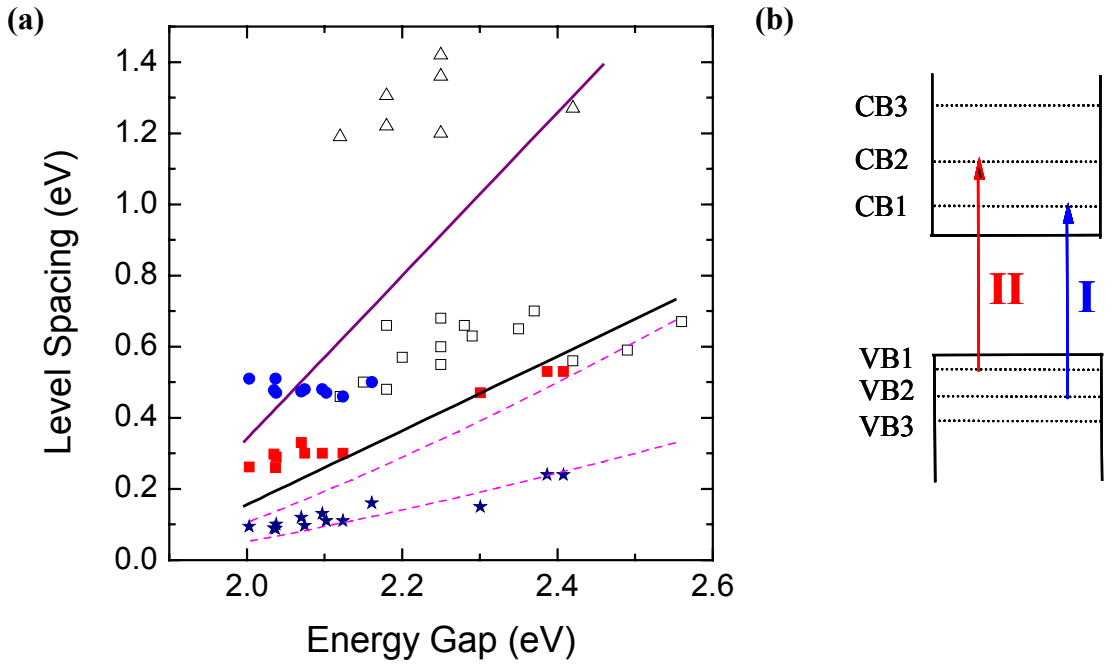

Figure 7. (a) Excited energy states versus energy gap. The respective separations between the tunneling peaks are denoted by open symbols. Spacing between the PLE transitions and the optical energy gap are presented by solid symbols. The calculated energy level separations are presented from bottom to top as follows: VB2-VB1, VB3-VB1 (dashed lines) and CB2-CB1, CB3-CB1 (solid lines). For the optical data, the energy gap was taken as the detection window corrected for the Coulomb interaction. The STM data represent 15 (out of 20) QRs whose spectra showed clear charging-free peak structure. (b) An illustration of the excited optical transition from different VBn states to CBn states.

This may be partly due to the oversimplified model, not taking into account the effect of the tip on the measured energy levels. In particular, the larger experimental level spacing as compared to theory may arise from the effect of voltage division as discussed above.

In most of our tunneling spectra, where charging effects were intentionally eliminated, each peak corresponds to resonant tunneling through a discrete energy level of the QR, as depicted in figure 4. In some cases however, we have acquired spectra with split CB peaks as shown in figure 8. The splitting may be attributed to the single electron charging effect as observed for QDs [2,9,12,14]. As demonstrated previously for QDs, the single electron tunneling (or peak) multiplicity can reflect the level degeneracy. The QR CB ground state is two-fold (spin) degenerate in agreement with the apparent charging doublet observed for the CB1 level in figure 8. However, the higher peaks also split into two while a four-fold degeneracy is expected for states with excited L_z levels [24]. This discrepancy may be due to partial charging or degeneracy lifting and further experiments are needed to resolve this issue. Note that the apparent band-gap in this spectrum is larger than that observed for the 4 nm diameter rod in figure 4(a). This is due to a combination of two effects. First, in order for charging effect to appear, the DBTJ should become more symmetric, thus further enhancing the effect of voltage division discussed above. Second, the single electron charging by-itself contributes to the gap enlargement [9, 14].

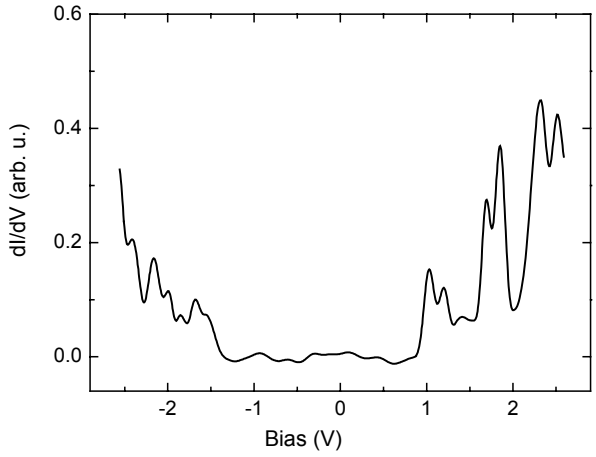

Figure 8. dI/dV versus V tunneling spectrum measured on a 25x4 nm QR. The doublets at positive bias are possibly due to single electron charging effects.

CONCLUSIONS

Combined optical and tunneling spectroscopy measurements provide a powerful tool for investigating the level structure of QRs. The experimental data obtained for CdSe QRs, both optical and tunneling, shows that the level structure is dominated by radius rather than by the length, and corresponds to model calculations with a good agreement. This behavior reveals the quasi one-dimensional nature of the QR even for aspect ratios as small as three with length above ~ 10 nm. Revealing QRs electronic properties allows one to select a desired QR length and tune its optical or electrical properties at will, using the diameter. This ability is of significant importance for future nanotechnology applications of QRs [4,27].

ACKNOWLEDGEMENTS

This work was supported in part by grants from the Bi-National Science Foundation, the DIP (Deutsche Israel Program) and the Israel Science Foundation.

REFERENCES

1. A. P. Alivisatos, *Science* **271**, 933 (1996).
2. O. Millo, D. Katz, Y. W. Cao, and U. Banin, *Phys. Rev. Lett.* **86**, 5751 (2001).
3. V. Klimov, A. Mikhailovsky, S Xu, A Malko, J.A. Hollingsworth, C.A. Leatherdale, H.J. Eisler and M.G. Bawendi ,*Science* **290** ,314 (2000).
4. M. Kazes, D. Y. Lewis, Y. Ebenstein, T. Mokari, and U. Banin, *Adv. Mater.* **14**, 317 (2002).
5. N. Tessler, V.Medvedev, M.Kazes, S. H. Kan, and U. Banin, *Science* **295**, 1506 (2002).
6. M. Bruchez, M. Moronne, P. Gin, S. Weiss and A.P. Alivisatos, *Science* **281**, 2013 (1998).

7. X .G. Peng, L Manna, W.D. Yang, J. Wickham, E. Scher, A. Kadavanich and A.P. Alivisatos, *Nature* (London) **404**, 59 (2000).
8. J. T. Hu, L.S. Li, W.D. Yang, L. Manna, L.W. Wang and A.P. Alivisatos, *Science* **292**, 2060 (2001).
9. U. Banin, Y. W. Cao, D. Katz, and O. Millo, *Nature* (London) **400**, 542 (1999).
10. D. J. Norris and M.G. Bawendi, *Phys. Rev. B* **53**, 16338 (1996).
11. U. Banin, C.J. Lee, A.A. Guzelian, A.V. Kadavanich, A.P. Alivisatos, W. Jaskolski, G.W. Bryant, A.l. Efros and M. Rosen, *J. Chem. Phys*. **109**, 2306 (1998).
12. E. P. A. M. Bakkers and D. Vanmaekelbergh*, Phys. Rev. B* **62**, R7743 (2000).
13. E. P. A. M. Bakkers, Z. Hens, A. Zunger, A. Franceschetti, L.P. Kouwenhoven, L. Gurevich and D. Vanmaekelbergh, *Nano Lett.* **1**, 551 (2001).
14. D. Katz, O. Millo, S. H. Kan, and U.Banin, *Appl. Phys. Lett.* **79**, 117 (2001).
15. A. Franceschetti and A. Zunger, *Phys. Rev. B* **62**, 2614 (2000).
16. Y. M. Niquet, C. Delerue, G. Allan and M. Lannoo, *Phys. Rev. B* **65**, 165334 (2002).
17. A. I. Ekimov, F. Hache, M.C. Schanneklein, D. Ricard, C. Flytzanis, I.A. Kudryavtsev, T.V. Yazeva, A.V. Rodina and A.L. Efros, *J. Opt. Soc. Am. B* **10**, 100 (1993).
18. X. Z. Li and J. B. Xia, *Phys. Rev. B* **66**, 115316 (2002).
19. J. T. Hu , *J. Phys. Chem*. **106**, 2447 (2002).
20. L. Manna, E. C. Scher, and A.P. Alivisatos, *J. Am. Chem. Soc*. **122**, 12 700 (2000).
21. Z. A. Peng and X. Peng, *J. Am. Chem. Soc.* **123**, 1389 (2001).
22. M. Tews, and D. Pfannkuche, *Phys. Rev. B* **65**, 073307 (2002).
23. L. S. Li, J. T. Hu, W. D. Yang, and A. P. Alivisatos, *Nano Lett*. **1**, 349 (2001).
24. P. C. Sercel and K. J. Vahala, *Phys. Rev. B* **42**, 3690 (1990).
25. D. Katz, T. Wizansky, O. Millo, E. Rothenberg, T. Mokari, and U. Banin, *Phys. Rev. Lett*. **89**, 86801 (2002).
26. L. E. Brus, *J. Chem. Phys.* **9**, 4403 (1984).
27. W. U. Huynh, J. J. Dittmer, and A. P. Alivisatos, *Science* **295**, 2425 (2002).